RSC Advances




ROYAL SOCIETY OF CHEMISTRY

www.rsc.org/advances

# The Enhancement of Liquid-Liquid Extraction with High Phase Ratio by Microfluidic-Based Hollow Droplet

Wen-Ting Wang, Fu-Ning Sang, Jian-Hong Xu,* Yun-Dong Wang, and Guang-Sheng Luo

We developed a novel method to enhance the liquid-liquid extraction with high phase ratio by a microfluidic-based hollow droplet structure. A one-step microfluidic capillary device is used for the generation of gas-in-oil-in-water double emulsions. The overall volumetric mass transfer coefficients increases about 10~60 times when gas bubbles are introduced. This method has potential applications in analytical chemistry, micro-extraction, biological extraction, and so on.

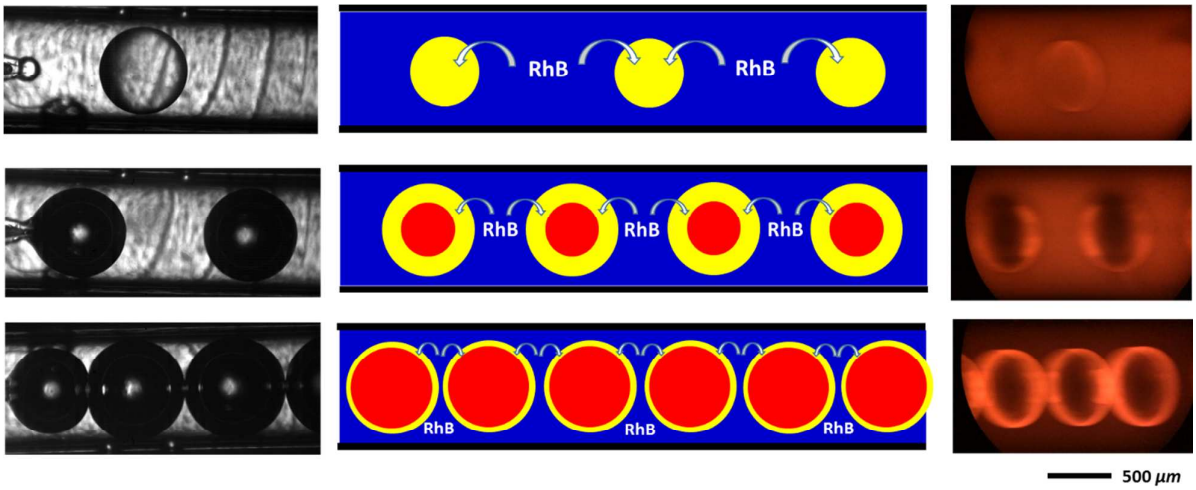

Journal Name

ARTICLE

# The Enhancement of Liquid-Liquid Extraction with High Phase Ratio by Microfluidic-Based Hollow Droplet†

Received 00th January 20xx,
Accepted 00th January 20xx

DOI: 10.1039/x0xx00000x

www.rsc.org/

Wen-Ting Wang, Fu-Ning Sang, Jian-Hong Xu,* Yun-Dong Wang, and Guang-Sheng Luo

In this work, we developed a one-step microfluidic capillary device for the enhancement of mass transfer process with high phase ratio by hollow droplet. Here we used a fluorescent material rhodamine B as the transportation substance which transfers from aqueous phase to oil phase. The qualitative demonstrations of extraction process have been presented. During the droplet formation stage, the fluorescent brightness of the droplets becomes more and stronger for droplet with and without a bubble in it. During the droplet moving stage, for both flow conditions, the fluorescence intensity increases along the out-let channel. At the latter half of the out-let channel, the addition of gas greatly enhances mass transfer process. The mean overall volumetric mass transfer coefficients $k_L a$ increases with the increase of gas flow rates, majorly because of the sharply raised specific area. And $k_L a$ of gas-liquid-liquid hollow droplet flow increases around 10~60 times compared to that of liquid-liquid droplet flow system. The length of extraction equipment needed to reach 95% extraction efficiency reduced around 10~1000 times when gas microbubbles is introduced. Based on the experimental data, a theoretical model has been built up for the potential prediction of the enhancement of extraction by adding gas microbubbles. Effective diffusion coefficient is introduced to combine the convective mass transfer factor into this model. The modeling results fit well with the experimental data. All the above results present a practical method for the enhancement of extraction process with high phase ratio systems, which has potential applications in analytical chemistry, micro-extraction, biological extraction, and so on.

## Introduction

Liquid-liquid extraction technology is an important separation unit and it is widely applied in many fields, such as chemical engineering, biology, material fabrication and analytical chemistry. However, in chemical industry, tradition extraction equipment have limited extraction capability with particular extraction systems. It always leads to large-scale volumes of equipment and very large cost of energy, as we always see in the chemical factories. The development of novel extraction equipment is very important for the chemical industry and environment protection.

Recently, liquid-liquid extraction based on microfluidic technology has been developed rapidly not only because of the reduction of the sample and portability, but also the better mass transfer performance than it is in conventional equipment such as extraction column, Mixer-settler, etc. For example, Burns et al. [1] developed a multiphase micro reactor based upon the use of slug flow through a narrow channel. The internal circulation was found to be the main reason for a large enhancement in the interfacial mass transfer from aqueous phase to oil phase. The experimental data showed a better extraction performance with microfluidic-based slug flow than conventional extraction methods. Kashid et al. [2] investigated the mass transfer performance of slug-flow for various operating conditions in a capillary microstructured reactor. Compared to conventional contactors, the mass transfer coefficients were approximately one order of magnitude higher allowing the process intensification. The results obtained demonstrate the benefits of microstructured reactors and confirm that the throughput of conventional reactors can be achieved. Pascaline et al. [3] analysed the extraction performance of fluorescein and rhodamine in drop flow and the influences of different parameters on process have been discussed. Xu et al. [4] studied the enhancement of the mass transfer performance by droplet flow in co-flowing microchannel. The data has been obtained by monitoring the extraction of succinic acid from n-butanol to aqueous drops containing *NaOH*. The mass transfer rate was 10-1000 times higher comparing to the traditional liquid-liquid systems. The results from this study indicate that droplet flow within micro

[a] *The State Key Lab of Chemical Engineering, Department of Chemical Engineering, Tsinghua University, Beijing 100084, China. E-mail: xujianhong@tsinghua.edu.cn. Tel: +86-10-62773017. Fax: +86-10-62773017.*

† Electronic Supplementary Information (ESI) available: See DOI: 10.1039/x0xx00000x

meter scale environment offers a viable alternative for two-phase reaction or separation process. Benz et al. [5] developed a micro mixer arrays to evaluate the extraction performance of miniplant technology as an alternative to conventional stirring apparatuses. The work proved that micro mixer arrays are highly efficient apparatuses for extraction purposes. Despite the circulations in particular flow pattern, such as slug flow, there are other reasons for the enhancement of extraction in micro device. In micro mixer, the dispersed phase can form in much smaller droplets and thus they will have larger specific area and shorter mass transfer distance than in ordinary-size equipment, which leads to faster mass transport rate. So in microfluidic devices, it takes less time as less than 1s to achieve liquid-liquid extraction equilibrium, which means in industry, it is environmental friendly and takes less energy.

Based on these basic researches on the liquid-liquid extraction in microfluidic device, this new method has been applied in the extraction of compounds of biological relevance [6-13], metal ions [14-18] and other chemicals [19-24]. Wagli et al. [12] combined a microfluidic-based multiphase liquid-liquid extraction method to extract cocaine continuously from IR-light-absorbing saliva to an IR-transparent solvent. They succeeded in detecting cocaine in real saliva samples spiked with the drug and allowing real time measurements, which makes this approach suitable for point-of-care applications. Nam et al. [11] described the separation of live and dead cells of Chinese hamster ovary cells by a change of overall surface properties of animal cells such as hydrophobicity and surface net charge. In their work, all live cells were partitioned to PEG-phase flow at the junction of outlet microchannel, while most of the dead cells were kept on the inter-face flow at pH 6.6. Maruyama et al. [18] studied a three-phase flow in a microchannel on a glass microchip. They demonstrated that the conventional methodology for solvent extraction of metal ions is applicable to solvent extraction in a microchannel. And they succeeded in the selective separation of a targeted metal ion from an aqueous feed solution to a receiving phase within a few seconds by employing a liquid membrane formed in a microfluidic device.
However, for extraction processes with high phase ratio (usually higher than 10:1), which is far away from 1:1, such as oil refining processes [25], caprolactam extraction [26], phosphoric acid purification [27, 28], hydrogen peroxide extraction [29], and most of the micro-extraction processes [30], the mass transfer distance in continuous phase will be larger and the contact area between the two phases will decrease sharply as the phase ratio increase. Therefore external energy input is greatly needed for these high phase ratio extraction processes. The development of more efficient extraction method and equipment is needed to overcome the above difficulties caused by high phase ratio. Tan et al. [31] designed a gas-agitated method for the intensification of $H_2O_2$ extraction with high phase ratio, which is larger than 50:1. A device with microfiltration membranes as the dispersion medium was developed to generate the gas-liquid-liquid micro dispersed system. The research results show that the overall volume mass transfer coefficient could be 10-30 times larger than the extraction process without gas addition. However, the detail structure of gas-liquid-liquid system during the extraction process has not been presented, and the mechanism of the enhancement of extraction by adding gas has not been systematically analysed.

In this work, we used a simple one-step microfluidic device for the formation of gas in oil in water dispersed system (also means hollow droplet structure) to realize the enhancement of extraction process from aqueous phase to oil phase with high phase ratio. A stable gas-in-oil-in-water hollow droplet structure (usually called double emulsions) can be easily fabricated with this microfluidic device. In our previous work [32-35], we have systematically analysed the generation of gas-in-liquid-in-liquid double emulsions and the structure control by changing system properties and operating conditions, as well as the formation mechanism of this kind of double emulsions. And these previous works have made a good foundation for this work on the enhancement of extraction behaviour of the hollow droplet structure. Herein, we used a fluorescent material rhodamine B as the transportation substance which transfers from aqueous phase to organic phase duo to the contrast in its chemical potential between the two phases. The qualitative and quantitative demonstrations of the enhancement of extraction process have been presented. The effects of equipment length, gas phase flow rates and phase ratios on the extraction process have been systematically studied and analysed. The mass transfer coefficients when extraction efficiency is 95% are calculated and discussed. Based on the experimental data, a theoretical model has been built up for the prediction of the enhancement of extraction by this kind gas filled hollow droplet.

## Experimental

### Microfluidic device

The experimental set-up is shown in Fig.1. The most important part of this device is the dual-coaxial capillary structure, where the oil droplet with a gas bubble inside it (gas-in-oil-in-water hollow droplet structure) is formed by the shearing force of continuous aqueous phase flow (Supporting Information MOV1). To fabricate this device, a smaller capillary is injected into another capillary and the tapered orifices are aligned where the one-step emulsification carries on, as the image shown in the rectangle with green dotted sides in Fig. 1. A circular glass capillary with inner-diameter of 0.70 *mm* and outer-diameter of 1.00 *mm* is tapered using a micropipet puller (P-97, SUTTER Co. Ltd., USA) for the injection of the gas phase fluid. The diameter of the tapered orifice is approximately 20 $\mu m$. The first tapered capillary is inserted into another capillary with inner-diameter of 1.05 *mm* and outer-diameter of 1.50 *mm* for the middle phase and the orifice is tapered to approximately 250 $\mu m$. We make sure that both the orifices align in the same plate. Then, these compound capillaries are inserted into the out-let channel, a third coaxially aligned capillary. The inner-diameter of the third capillary is 1.05 *mm* and the outer-diameter is 1.5 *mm*. We changed the length of the out-let channel to control the

residence time of the two liquid phases. The capillaries are fixed on a Cross-junction channel which is fabricated on a polymetyl methacrylate (PMMA) plate using a Computerized Numerical Control (CNC) machine tool with an end mill (Φ = 1.0 *mm*). The channels for dispersed phase fluid and the continuous phase fluid are both approximately 1.5 *mm* wide × 1.5 *mm* high. PTFE pipes are inserted into the in-let channel and micro syringe pumps (LSP01-1B, Baoding Longer Precision Pump Co., Ltd) are used to pump the gas phase and two liquid phases into the microfluidic device. The outlet channel, the phase separator made by a silicon tube with $\emptyset = 6\ mm \times 7\ mm, h = 8\ cm$ , and the exit made by a glass capillary with inner-diameter of 1.05 *mm,* make up a T union, which is fixed on a T -junction channel fabricated on another PMMA plate. All the three phases flow through the outlet channel, into the separator. The phase separation is achieved by density difference of three phases. The phases with low density, oil phase and gas phase, float up to the top surface of the separator. The oil phase accumulates on the top surface and can be pumped out into the sample reservoir. The gas phase escapes into the air atmosphere as soon as it gets into touch with the atmosphere. As gas is much lighter than liquid, the addition of gas can intensify the phase separation process. The high-density continuous aqueous phase, however, flows past the separator, straight to the exit, which is at the bottom of the separator. And then the aqueous phase can be collected in the sample reservoir.

The experimental process is operated under a fluorescent microscope (DSU, Olympus) with 450 *nm*-650 *nm* UV as the exciting light of rhodamine B, and the flow condition and the fluorescence intensity of the out-let flow is observed by a high-speed video camera (Phantom 663, 2500 fps) mounted on the microscope.

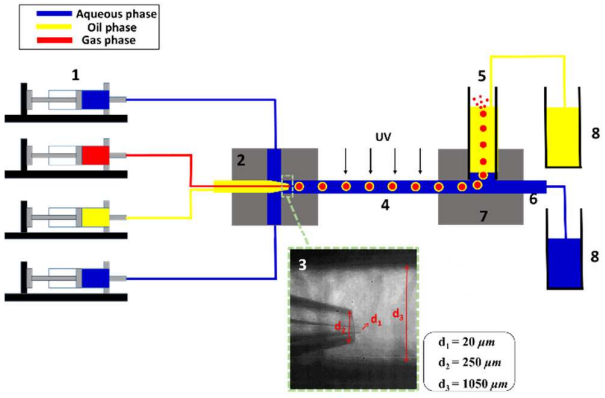


1 Pump 2 Cross-junction channel 3 dual-coaxial capillary 4 Out-let flow channel
5 Phase separator 6 exit 7 T-junction channel 8 Liquid sample reservoir

Fig.1 The structure of the microfluidic device.

### Materials

In our experiments, the air gas, as the inner phase, breaks up into microbubbles at the orifice, and dispersed into the oil phase (49 *wt*.% silicon oil (10 *cst*) + 49 *wt*.% octanol+2 *wt*.% *Dowcorning 749*). And then, the oil droplets encapsulating a gas bubble each are sheared off by the outer aqueous phase flow, which contains 2.5 *wt*.% polyethylene glycol and rhodamine B (95%, J&K) in concentrations of 10.0 *mg/L.* The distribution coefficient of rhodamine B between the oil and aqueous phase is 46, which is obtained from our extraction experimental data with shake flasks. And the viscosity of the aqueous phase is 2.60 *mPa s*, which is measured by a rotor viscosity meter (LVDV- II +PRO, *Brookfild*). The surface/interfacial tensions of gas-aqueous, gas-oil, aqueous-oil are 50.46 *mN/m*, 23.42 *mN/m*, 7.85 *mN/m* respectively, which indicate that the gas-in-oil-in-water double emulsions will be a thermodynamically steady structure[36] .

### Analysis

Two kinds of experimental results have been obtained from the analysis, qualitative ones and quantitative ones. The qualitative results means the fluorescence intensity of the oil droplets, which can be observed from the fluorescent microscope. As rhodamine B transported from the aqueous phase to the organic phase, the concentration of rhodamine B in oil phase increases along the out-let flow channel. According to Beer-Lambert Law, the fluorescence intensity is linear to the concentration of rhodamine B when it is at low concentrations. Therefore, the fluorescence intensity increases along the out-let flow channel.

The quantitative results are obtained by measuring concentrations of the aqueous phase samples collected after the phase separation reservoir. A UV-visible spectrophotometer (UV-2450, Shimadzu) is used to measure the concentration of rhodamine B in aqueous phase. According to the spectrum (Fig. 1 in Supporting Information), the maximum absorption wavelength of rhodamine B is 550 *nm*. And the standard curve (Fig. 2 in Supporting Information) shows that the absorbance is linear to the concentration when it is below 20 *mg/L*.

## Theoretical background

### Mass transfer equation

In extraction process, the mass transfer resistances can be presented in the form of equation 1[37, 38]

$$\frac{1}{k_L} = \frac{1}{Kk_d} + \frac{1}{k_c} \quad (1)$$

where $k_L, k_d, k_c$ are the mass transfer coefficient of overall system, dispersed phase and continuous phase respectively, $s^{-1}$. $\frac{1}{k_L}, \frac{1}{k_d}, \frac{1}{k_c}$ are the mass transfer resistance of overall system, dispersed phase and continuous phase respectively. K is the distribution coefficient of dispersed phase and continuous phase.

When $K \ll 1$, the mass transfer resistance in the dispersed phases is much larger than that of continuous phase, so that the resistance in continuous phase can be ignored. And the overall mass transfer coefficient $k_L = Kk_d$. When $K \gg 1$, on the contrary, $k_L = k_c$. For our experimental system, $K = 46 \gg 1$, so the overall mass transfer coefficient $k_L = k_c$. In other words, in our experiments, the resistance in dispersed phase is ignored and we consider that the concentration in dispersed phase becomes uniform instantly.

**Mass transfer model for the continuous phase fluid**

From the above analysis, only mass transfer performance outside the droplets is taken into account in our extraction system. Sherwood number ($Sh = kd/D$) is always called dimensionless mass transfer coefficient, which is the ratio of convective mass transfer to the molecular diffusion. For fully developed velocity and concentration profiles, *Sh* becomes constant and the mass transfer coefficient is inversely proportional to characteristic length *d*. There are several models predicting *Sh* outside the droplets which are summarized in different operating conditions in fully developed flow. The applicability of these models depends on the Peclet number ($Pe = ud/D$, $u$ is the the relative velocity of the continuous phase and a dispersed phase, *m/s*) and Reynolds number ($Re = \rho du/\mu$, $\rho$ and $\mu$ are the density and viscosity of the continuous phase, $kg/m^3$ and $Pa \cdot s$).

For the condition[39] where the continuous phase is still, $Sh_0$ = 2. This is the minimum value of *Sh* outside the droplets and the applicable condition is $Pe \rightarrow 0$.

For the conditions[40] where the continuous flow pattern is creeping flow and $Re \leq 1, Pe \gg 0$

$$Sh_c = 1 + (1 + 0.564Pe^{2/3})^{3/4} \quad (2)$$

For the conditions[41] when $Re > 1$

$$Sh_c = 2.0 + 0.76Re^{1/2}Sc^{1/3} \quad (3)$$

where $Sc = \mu/\rho D$, represents the ratio of viscous diffusion rate to the molecular diffusion.

## Results and Discussion

**Qualitative Analysis.**

With the observation of fluorescent microscope, the mass transfer from the continuous aqueous phase to the oil droplets along the out-let channel can be qualitatively demonstrated. The extraction process can be divided into two steps: droplets formation stage and droplet moving stage.

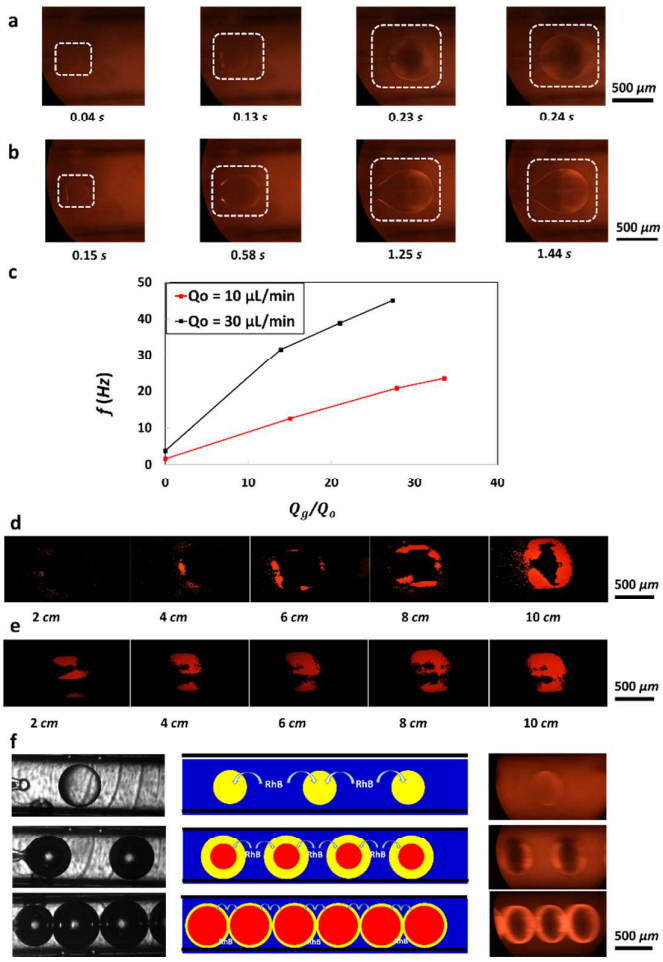


Fig. 2 a) Fluorescence images during droplet formation stage with microbubble inside it. The dotted outlines highlight the droplets ($Q_a = 600\ \mu L/min$, $Q_o = 6\ \mu L/min$, $Q_g = 16\ \mu L/min$). b) Fluorescence Images during droplet formation stage without microbubble ($Q_a = 600\ \mu L/min$, $Q_o = 6\ \mu L/min$ and $Q_g = 0\ \mu L/min$). c) The generation droplet formation frequency with different gas phase to oil phase ratios. $Q_a = 600\ \mu L/min$. d) Fluorescence images of gas-in-oil-in-water flow conditions at different locations of the out-let channel during droplet moving stage ($Q_a = 600\ \mu L/min$, $Q_o = 6\ \mu L/min$, $Q_g = 16\ \mu L/min$). e) Fluorescence images of liquid-liquid flow conditions at different locations of the out-let channel during droplet moving stage ($Q_a = 600\ \mu L/min$, $Q_o = 6\ \mu L/min$ and $Q_g = 16\ \mu L/min$). f) The images on the left show the different generation frequencies when the inner gas flow rates are increased from 0 to a high value. In the middle are the sketch of dispersion states inside the out-let channel before and after gas microbubble is introduced. The images on the right show the increase of fluorescence intensity when the gas phase is added.

**Droplets formation stage**

The extraction performances within the droplets formation stage are shown in Fig. 2a, b and MOV2, MOV3 in Supporting Information. The aqueous and organic flow rates are 600 $\mu L/min$ and 6 $\mu L/min$ respectively both for the two operating conditions, and for MOV3 there is additional gas flow with the flow rate of 16 $\mu L/min$. We can see that for both operating conditions(MOV2, MOV3 and dotted outlines in Fig.2 a & b), it is obvious that as the droplet grow up at the tip of the capillary, the fluorescent brightness of the droplets becomes more and more strong. This is because as long as the two phases get into touch, rhodamine B starts to transport from the continuous aqueous phase into the oil phase droplet. The brightness starts at the edges of the droplet, and then spreads inside the droplets. Since the distribution coefficient is a relatively high value, 46, the brightness inside dispersed liquid phase and at the edge of the phase interfaces could be much higher than in the continuous phase when the transformation occurs. Because the mass transfer between the two liquid phases happens at the phase interface, the brightness of the interface should be light up firstly, and also strongly. And this is why the edge of the droplet is so clear. In the dotted rectangle in the Fig. 2a&b, the bright areas of the phase interfaces and within the droplets represent the location where Rhodamine B molecules are. The brighter the area is, the higher the Rhodamine B concentration is. So we can qualitatively infer the fluorescence intensity and the Rhodamine B concentration by the brightness of the droplet. For the droplets without a bubble, we can also observe the fluorescent brightness spreads along two incomplete arcs, which are symmetrical to the axis of the droplets (Fig. 2b). This phenomenon could be explained by the inner loop of the droplets during the formation process. And this internal circulation is the main factor that increase the extraction rate. For the gas-in-oil hollow droplets, the generation frequency ( $f$ ) is higher than simple droplets (Fig. 2c). During the formation stage, the oil phase first flow out of the annulus of the two capillary tips, and when the oil sphere grows to a certain size, the gas phase bubble out of the inner capillary tip and then the whole hollow droplet is sheared off by the outer phase flow. Because of the additional bubble, there's no internal circulation in the organic phase and the total fluorescence lightness is weaker than the simple oil droplet during the droplet formation stage. The gas phase has no fluorescence response to the UV light, therefore a black round could be observed when the gas bubble is introduced (Fig. 2a).

**Droplet moving stage**

For the qualitative demonstration during droplet moving stage in the out-let channel, MOV4 and MOV 5 in Supporting Information show the videos of two flow conditions, which are captured at the same location, 10 *cm* away from the dispersing point. The aqueous and oil flow rates are 600 *μL/min* and 6 *μL/min* respectively both for the two conditions, and for MOV5 there is additional gas flow with the flow rate of 16 *μL/min*. Fig. 2d and 2e show the fluorescence images of two flow conditions at different locations of the out-let channel. In order to enhance the visual contrast, we treated the original pictures with deduction of background's grayscale, and the image processing method is shown in the Supporting Information. The figures below the images represent the distance away from the droplet formation tip, and the flow rates are $Q_a = 600\ \mu L/min$ , $Q_o = 6\ \mu L/min$ for both conditions and $Q_g = 16\ \mu L/min$ for Fig. 2d (condition A), $Q_g = 0\ \mu L/min$ for Fig. 2e (condition B). We can see that for both flow conditions, the fluorescence intensity increases along the out-let channel because of the transport of rhodamine B into droplets as the contact time of two phases lasts. At the location of 2 *cm*, the fluorescence intensity of condition B is higher than condition A, this is because this location is not far away from the droplet formation stage, after which the extraction performance of single oil droplets is better than that of gas-in-oil hollow droplets. However, as the flow continues, for example at the points of 6 to 8 *cm*, the fluorescence intensity of condition A becomes higher than condition B, which means the total extraction performance of condition A is better. For the first reason, the internal circulation inside simple oil droplet disappears after the droplet breakup at the capillary tip, and the enhancement of mass transfer by the internal circulation disappears either. For the second reason, as shown in Fig. 2f, with the addition of microbubble inside the oil droplet shortened the mass transfer distance in oil phase because the oil droplet becomes a thin oil membrane spreading on the surface of microbubble. And the mass transfer distance shortens from the radius of the droplet (around 350 $\mu m$) to the thickness of the thin membrane (around 20 $\mu m$). For the third reason, the mass transfer distance in aqueous phase is shortened largely. When gas phase is introduced, the generation frequency increases, therefore the space interval of every two droplets decreases, and the most of the rhodamine B molecules can travel a shorter distance to reach the interfaces of two phases. For the fourth reason, the contact area of two liquid phases also increases as the droplets becomes denser when the gas microbubble is added.

**Quantitative Analysis**

In order to get the specific extraction performance of the two flow conditions, the concentrations of rhodamine B during the extraction process must be obtained. We get the accurate data by analysing the concentrations of aqueous phase samples collected after the micro- phase separator, as shown in Fig. 1. We change the length of out-let channel from 5 *cm* to 30 *cm* with intervals of 5 *cm* for different residence time. We define extraction efficiency E as Equation 4.

$$E = (C_0 - C_{ext})/(C_0 - C^*) \quad (4)$$

$$Q_a C_0 + Q_o \times 0 = Q_a C^* + Q_o K C^* \quad (5)$$

Where $C_0$ is the initial concentration of rhodamine B in aqueous phase, *mg/L*. $C_{ext}$ is the concentration of the out-let collected aqueous sample, *mg/L*. $C^*$ is the equilibrium

concentration, *mg /L*, which can be calculated by Equation 5. $Q_a$ and $Q_o$ are the flow rate of aqueous phase and oil phase respectively. $K$ is the distribution coefficient of rhodamin B between the oil and aqueous phase. In our experimental system, $K$ is 46. Fig. 3a-d show the extraction efficiency changes along the out-let channel for different operating conditions. *L* is the distance from sampling point to the capillary tip, *cm*. Fig. 3a shows that when the aqueous to oil phase ratio is at a high value of 100:1, *E* increases from <40% to >95% with the increase of inner gas flow rate, which indicates that the mass transfer rate is highly increased. Fig. 3b, 3c &3d show that when the aqueous to oil phase ratios are at a relatively lower value, 59:1, 40:1 and 20:1, *E* increases sharply as long as the gas phase is introduced. However, when the gas phase flow rate increases, *E* only tends to increase in a small range, which is within 10% in our operating conditions. This is probably because the different gas phase rate ranges among different aqueous to organic phase ratios. As the oil phase flow rate increases, it tends to hold a relatively high gas flow rate in order to stable the flow. For example, the gas flow rate ranges from 180 $\mu L/min$ to 500 $\mu L/min$ for Fig. 3a, and it ranges from 250 $\mu L/min$ to 600 $\mu L/min$, 250 $\mu L/min$ to 700 $\mu L/min$ and 700 $\mu L/min$ to 1400 $\mu L/min$ for Fig. 3b, 3c & 3d, respectively. As shown in Equation 6, when $Q_g$ is high enough matching $Q_a$, higher gas phase ratio easily makes a faster droplet moving velocity, which leads to a shorter residence time at the same out-let channel length. As the residence time decreases, *E* can't increase obviously even though more gas is introduced.

$$u = (Q_a + Q_o + Q_g)/A \quad (6)$$

where *u* is the average velocity of the three phases, *m/s*. *A* is cross sectional area of the out-let channel, $m^2$.

The mean overall volumetric mass transfer coefficients ($k_L a, s^{-1}$) are usually used to represent the mass transfer characteristics in microchannels. $k_L a$ can be calculated by the following equations:

$$Q_a(C_0 - C_{ext}) = k_L a V \overline{\Delta C} \quad (7)$$

$$a = 6\varphi/d_{droplet} \quad (8)$$

$$\varphi = (Q_g + Q_o)/(Q_g + Q_o + Q_a) \quad (9)$$

$$\overline{\Delta C} = [(C_0 - C_0^*) - (C_{ext} - C_{ext}^*)]/[ln(C_0 - C_0^*) - ln(C_{ext} - C_{ext}^*] \quad (10)$$

$$C_0^* = C_{m0}/K, C_{ext}^* = C_{mext}/K \quad (11)$$

$$Q_a C_0 + Q_o \times 0 = Q_a C_{ext} + Q_o C_{oext} \quad (12)$$

where *a* is the interfacial mass transfer area between the two liquid phases per unit volume of the microchannel, */m*, which can be obtained by Equation 8. $\varphi$ is the volumetric flow fraction of dispersed phases, which can approximately be calculated by Equation 9. *V* is the microchannel volume, $m^3$. $\overline{\Delta C}$ is the logarithmic mean concentration driving force, *mg/L*. $C_0^*$ is the equilibrium concentration of the solute in the inlet aqueous phase, corresponding to the actual inlet concentration of the solutes in the organic phase $C_{m0}$, which is 0. $C_{ext}^*$ is the equilibrium concentration of the solutes in the outlet aqueous phase, corresponding to the actual outlet concentration of the solutes in the organic phase $C_{mext}$, which can be calculated by the mass conservation Equation 12.

Here we choose the 30 *cm*- length microchannel as the overall volume. Fig. 3e shows that the mean overall volumetric mass transfer coefficients $k_L a$ increases with the increase of gas to oil phase ratio. When $Q_g/Q_o$ increases from 0 to 50, $k_L a$ becomes 2 to 10 times larger that that without gas phase. This is mainly because of the sharp increase of specific area when the gas microbubbles are introduced, which is demonstrated in Fig. 3f.

In order to compare the extraction performances when the flow and mass transfer is well developed， we discussed the mean mass transfer coefficient $k_L a$ which is obtained during the length interval, [0, $L_{95\%}$]. $L_{95\%}$ is the channel length needed for *E* to reach 95%. Equation 7 to 12 with some detailed correction can be applied to this calculation, where $C_{95\%}$ is instead of $C_{ext}$ and $AL_{95\%}$ is instead of *V*. $C_{95\%}$ is the concentration in aqueous phase when *E* = 95%, which can be calculated by equation 4 and 5. *A* is the cross-sectional area of the out-let channel, $m^2$. $L_{95\%}$ is a value obtained by an experimental data fitted equation when *C* get to $C_{95\%}$. Here an exponential function[3] $C = M + Nexp(-PL)$ is applied to fit the experimental data. M, N and P are undetermined constants and M, N are related to the concentrations of the inlet and outlet aqueous flow. The data of C and L in the range of [0, 30 *cm*] are used to fit the exponential function in different operating conditions.

Fig. 3g-i show the results of $L_{95\%}$, $k_L a$ and $k_L$. $k_L$ is calculated by the equation $k_L = k_L a/a$. From Fig. 3g, we can see that the length of extraction equipment needed to reach 95% extraction efficiency reduced around 10~1000 times when gas microbubbles is introduced. It means that when a specific extraction efficiency is wanted, the addition of gas can largely reduce the equipment size and even shorten the extraction time, not only because of the shorter length of out-let channel but also the higher move velocity. And as shown in Fig. 3h, $k_L a$ of gas-liquid-liquid hollow droplet flow increases around 10~60 times compared to that of liquid-liquid droplet flow system. The sharply increased specific area is the major contribution to this enhancement of extraction performance. And the mass transfer coefficient $k_L$ is also a contribution, as shown in Fig. 3i. $k_L$ increases around 2 ~ 3 times when gas phase is added. This phenomenon can roughly be explained by the two-film theory model[38], where $k_L = D/\delta$ is presented. When the gas phase is introduced, the interval between two droplets decreases, which leads to the decrease of concentration boundary layer $\delta$ and increase of $k_L$.

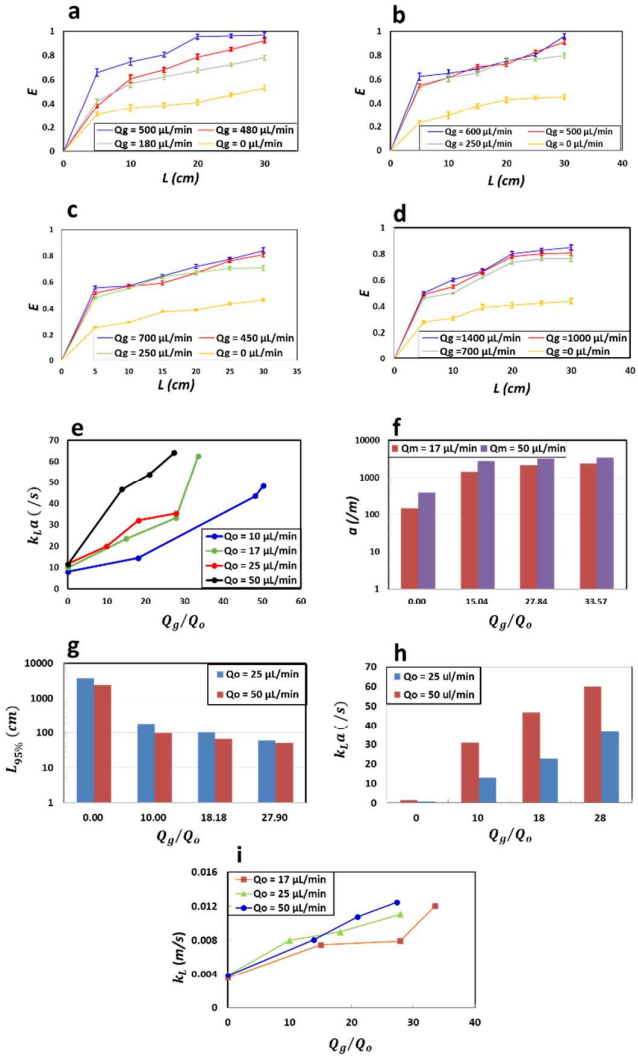


Fig. 3 a, b, c, d) The influences of Q_g and L on the extraction efficiency when Q_o=10,17,25,50 µL/min respectively. The RSDs are less than 5%. e) The influence of gas to oil phase ratio Q_g/Q_o and oil phase flow rate Q_o on k_L a. f) The specific area a variation as the increase of Q_g/Q_o (Q_o=17 µL/min and 50 µL/min ). g, h, i) The variation of L_(95%),k_L a and k_L respectively when E = 95% in different operating conditions. All the above data are obtained on the condition of Q_a=1000 µL/min.

## Theoretical model

In order to further analyse the mechanism of enhancement of extraction process with the introduction of gas microbubbles, a theoretical model is built. Due to the steady flow condition, the mass transfer process in the out-let channel is divided into quantities of same separate unites (as shown in Fig. 4, inside red dotted rectangle). Each unit of gas-liquid-liquid fluid can be simplified into a sphere which contains a gas bubble in the centre and two liquid films spreading outside the bubble orderly. The oil film is at the middle of the gas bubble and the aqueous film (Fig. 4a). Each unit of liquid-liquid flow can be simplified into a sphere which contains an oil droplet in the centre and an aqueous film spreading on it. In the extraction process, the rhodamine B molecule transfers from the aqueous phase to the organic phase.

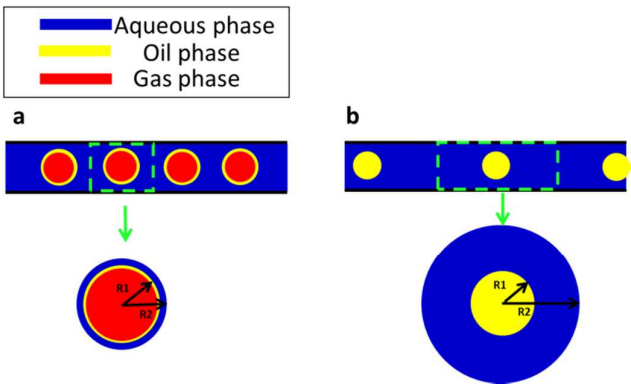


Fig. 4 Schematic representation of the mass transfer unit in G/O/W system and O/W system.

The following assumptions are made for the modelling of mass transfer process.

1) The process is based on diffusion model. The effective diffusion coefficient is used to combine the convective mass transfer factor into this model. The effective diffusion coefficients can be calculated by Equation 13.

$$D_{eff} = K_f D \quad (13)$$

where $D$ is the diffusion coefficient. From Culbertson et al.'s research[42] and Wilke-Chang model[43], we could get $D = 1.8 \times 10^{-10}\ m^2/s$. $K_f$ is the mass transfer strengthening factor, which is defied by Equation 14.

$$K_f = Sh_c/Sh \quad (14)$$

As stated in theoretical background part, $Sh_0 = 2$. The formula of $Sh_c$ is depend on $Re$. Fig. 5a shows the $Re$ values in different operating conditions. For liquid-liquid flow, $Re < 1$, and Equation 2 is applied to calculate $Sh_c$. While for gas-liquid-liquid flow, $Re > 1$, so Equation 3 is applied. The effective diffusion coefficient is presented in Fig. 5b. $D_{eff}$ for liquid-liquid flow arranges from $6 \times 10^{-9}\ m^2/s$ to $7 \times 10^{-9}\ m^2/s$, and that for gas-liquid-liquid flow arranges from $8 \times 10^{-9}\ m^2/s$ to $1 \times 10^{-8}\ m^2/s$. $K_f$ is ranged from 30 to 60.

2) The overall radius $R_2$ can be calculated by the droplet radius $R_1$ as well as the flow rate ratio (Equation 15). $R_1$ can be measured with the captured images in our experiments.

$$\left(\frac{R_1}{R_2}\right)^3 = \frac{Q_o+Q_g}{Q_o+Q_a+Q_g} \quad (15)$$

3) The mass transfer resistance in oil phase is ignored according to Equation 1 in the section of theoretical background. In addition, the thickness of oil film is considerably small compared to aqueous film. Therefore, the concentration in organic phase is considered uniform.
4) The mass transfer resistance at the aqueous-oil interface is ignored and the concentration at the interface is consistent with distribution coefficient.
5) There's no mass transfer between every two neighbouring unites since they are totally equivalent.
6) Spherical coordinate is used and there's only mass transfer in the direction of *r* but no mass transfer in the other two directions.

With all the above assumptions, mass transfer through the aqueous film can be approximately described using Continuum Model in the spherical coordinate, which is written as:

$$\frac{1}{D_{eff}}\frac{\partial C}{\partial t} = \frac{1}{r}\frac{\partial^2 (rC)}{\partial r^2} \quad (16)$$

where *C* is the concentration in aqueous phase according the position *r* and mass transfer time *t*.

Initial condition: $t = 0,\ R_1 \le r \le R_2,\ C = C_0$

Boundary conditions: $t > 0,\ r = R_2,\ \frac{\partial C}{\partial r} = 0$

$$\mathrm{r} = R_1,\ C = C_{it} = C_m/K \quad (17)$$

$C_0$ is the initial concentration in aqueous phase.
$C_m$ is the concentration in organic phase according *t*, which can be calculated by mass conservation equation :

$$Q_a \times C_0 = Q_a \times \bar{C} + Q_o \times C_m \quad (18)$$

$\bar{C}$ is the average concentration in aqueous phase according t:

$$\bar{C} = \frac{3}{4\pi({R_2}^3 - {R_1}^3)} \int_{R_1}^{R_2} 4\pi r^2 C dr \quad (19)$$

In the above model, $C_0$ and $R_1$ are given. We carried out the above model with numerical solutions by Matlab. Fig. 5c and 5d show the modelling results of extraction efficiency calculated by Equation 4, as well as the comparison with the experimental data. The length $L = u \times t$ and $u$ is given by Equation 6. The modelling results show good coincidence with experimental data. So it is feasible to predict the extraction performance by using this model. Fig. 5e and f are the results of prediction where the droplet size $R_1$ assumed to be 1 *mm* at all the operating conditions. Fig. 5e and f show that with high aqueous to organic phase ratio, the increase of gas to organic phase ratio leads to the increase of extraction efficiency in the same equipment volume. When the gas to oil phase ratio is higher than 100, it takes less than 10 *cm* length of equipment to complete extraction. This prediction may not fit well with some of the real results, because some operating limits are not taken into consideration, such as coalescence of microbubbles and the instability of flow condition when the gas to oil phase ratio is very high. However, it is still a practical model to obtain the approximate results within particular operating conditions.

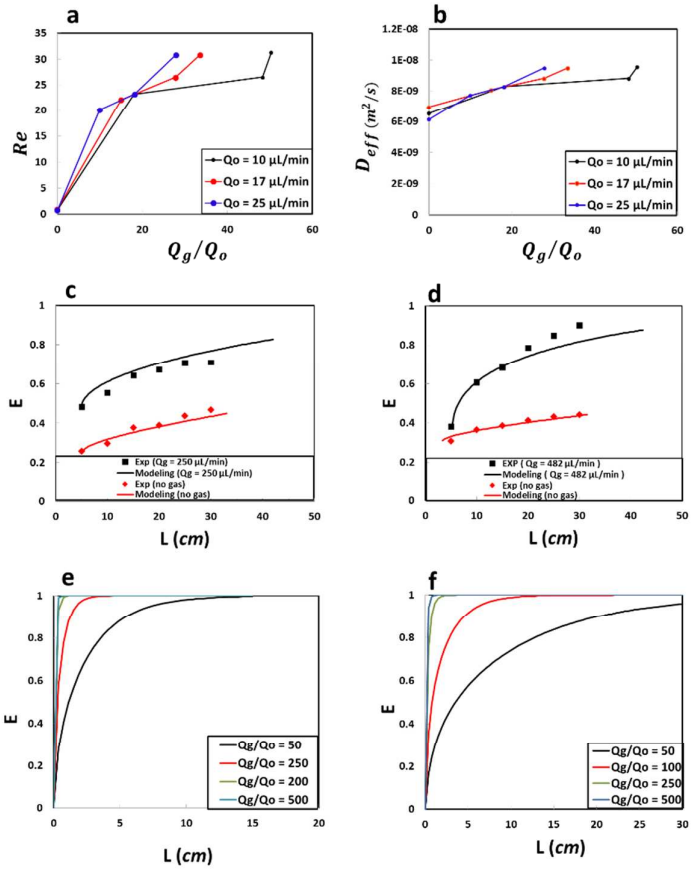


Fig. 5 a) The effect of Q_g/Q_o on Re. b) The effect of Q_g/Q_o on D_eff. c, d) The comparison of extraction efficiency between experiment values and modelling results for Q_a=1000 μL/min, Q_o=25 μL/minand Q_a=1000 μL/min, Q_o=10 μL/min respectively. e, f) The prediction of extraction efficiency on operating conditions of Q_a=1000 μL/min, Q_o=25 μL/min and Q_a=1000 μL/min, Q_o=17 μL/min, respectively.

## Conclusions

In this work, we used a one-step microfluidic capillary device to form Gas in oil in water dispersed system (also means hollow droplet structure) to realize the enhancement of mass transfer with high phase ratio by hollow droplet. Here we used a fluorescent material rhodamine B as the transportation substance which transfers from aqueous phase to oil phase. The qualitative demonstrations of extraction process have been presented. During the droplet formation stage, the fluorescent brightness of the droplets became stronger and

stronger for droplet. The inner convection inside the oil droplet was observed. During the droplet moving stage, for both flow conditions, the fluorescence intensity increased along the out-let channel, which is because more and more rhodamine B transports into droplets as the contact time of two phases lasts. At the latter half of the out-let channel, the fluorescence intensity of droplet with a microbubble inside it became higher than single droplet, which means the addition of gas microbubbles enhance the mass transfer process. The quantitative experimental results show the effects of equipment length, flow rates, phase ratios on the extraction efficiency. $k_L a$ is introduced to characterize the mass transfer rate. Within the equipment length of 30 *cm*, $k_L a$ increases with the increase of gas flow rates, majorly because of the sharply increased specific area. And $k_L a$ of gas-liquid-liquid hollow droplet flow increases around 10~60 times compared to that of liquid-liquid droplet flow system. The length of extraction equipment needed to reach 95% extraction efficiency reduced around 10~1000 times when gas microbubbles is introduced. Based on the experimental data, a theoretical model was built up for the potential prediction of the enhancement of extraction by adding gas microbubbles. Effective diffusion coefficient is introduced to combine the convective mass transfer factor into this model. The modelling results fit well with the experimental data. With this model, some predictions for the enhancement of extraction are made with different flow conditions. All the above results present a practical method for the enhancement of extraction process with high phase ratio systems, which has potential applications in different area including analytical chemistry, micro-extraction and biological extraction. For the use of this method, in order to get the stable gas-in-liquid-in-liquid flow condition, the interface tensions of three phases have to meet a particular condition which was stated by Torza[36] in 1969. For those systems that don't meet this condition, if it is allowed, surfactants can be used to adjust the interface tensions. However, for the particular systems that do neither meet this condition, nor allow additional surfactant, this method cannot be used because of the thermodynamic limitation.

## ACKNOWLEDGMENTS

The authors gratefully acknowledge the supports of the National Natural Science Foundation of China (21476121, 21322604) and Tsinghua University Initiative Scientific Research Program (2014z21026) for this work.

## REFERENCES

1. J. R. Burns and C. Ramshaw, *Lab Chip*, 2001, **1**, 10-15.
2. M. N. Kashid, A. Gupta, A. Renken and L. Kiwi-Minsker, *Chem Eng J*, 2010, **158**, 233-240.
3. P. Mary, V. Studer and P. Tabeling, *Anal Chem*, 2008, **80**, 2680-2687.
4. J. H. Xu, J. Tan, S. W. Li and G. S. Luo, *Chem Eng J*, 2008, **141**, 242-249.
5. K. Benz, K. P. Jackel, K. J. Regenauer, J. Schiewe, K. Drese, W. Ehrfeld, V. Hessel and H. Lowe, *Chem Eng Technol*, 2001, **24**, 11-17.
6. K. K. R. Tetala, J. W. Swarts, B. Chen, A. E. M. Janssen and T. A. van Beek, *Lab Chip*, 2009, **9**, 2085-2092.
7. G. Munchow, S. Hardt, J. P. Kutter and K. S. Drese, *Lab Chip*, 2007, **7**, 98-102.
8. Y. S. Huh, S. J. Jeon, E. Z. Lee, H. S. Park and W. H. Hong, *Korean J Chem Eng*, 2011, **28**, 633-642.
9. Y. S. Huh, C. M. Jeong, H. N. Chang, S. Y. Lee, W. H. Hong and T. J. Park, *Biomicrofluidics*, 2010, **4**.
10. M. C. Morales and J. D. Zahn, *Microfluid Nanofluid*, 2010, **9**, 1041-1049.
11. K. H. Nam, W. J. Chang, H. Hong, S. M. Lim, D. I. Kim and Y. M. Koo, *Biomed Microdevices*, 2005, **7**, 189-195.
12. P. Wagli, Y. C. Chang, A. Homsy, L. Hvozdara, H. P. Herzig and N. F. de Rooij, *Anal Chem*, 2013, **85**, 7558-7565.
13. P. Znidarsic-Plazl and I. Plazl, *Lab Chip*, 2007, **7**, 883-889.
14. O. Tamagawa and A. Muto, *Chem Eng J*, 2011, **167**, 700-704.
15. D. Tsaoulidis and P. Angeli, *Chem Eng J*, 2015, **262**, 785-793.
16. C. Priest, J. F. Zhou, S. Klink, R. Sedev and J. Ralston, *Chem Eng Technol*, 2012, **35**, 1312-1319.
17. D. Ciceri, L. R. Mason, D. J. E. Harvie, J. M. Perera and G. W. Stevens, *Microfluid Nanofluid*, 2013, **14**, 213-224.
18. T. Maruyama, H. Matsushita, J. Uchida, F. Kubota, N. Kamiya and M. Goto, *Anal Chem*, 2004, **76**, 4495-4500.
19. H. Shen, Q. Fang and Z. L. Fang, *Lab Chip*, 2006, **6**, 1387-1389.
20. S. A. Bowden, P. B. Monaghan, R. Wilson, J. Parnell and J. M. Cooper, *Lab Chip*, 2006, **6**, 740-743.
21. J. Hereijgers, N. van Oeteren, J. F. M. Denayer, T. Breugelmans and W. De Malsche, *Chem Eng J*, 2015, **273**, 138-146.
22. N. D. Raimondi, L. Prat, C. Gourdon and J. Tasselli, *Chem Eng Sci*, 2014, **105**, 169-178.
23. C. Priest, M. D. Reid and C. P. Whitby, *J Colloid Interf Sci*, 2011, **363**, 301-306.
24. Z. Barikbin, M. T. Rahman, P. Parthiban, A. S. Rane, V. Jain, S. Duraiswamy, S. H. S. Lee and S. A. Khan, *Lab Chip*, 2010, **10**, 2458-2463.
25. P. M. Nesterov, V. V. Kafarov and Shestopa.Vv, *Ind Lab+*, 1967, **33**, 83-&.
26. X. C. Gong, Y. C. Lu, Z. X. Qian and G. S. Luo, *Ind Eng Chem Res*, 2009, **48**, 4507-4513.
27. H. Ahmed, H. Diamonta, C. Chaker and R. Abdelhamid, *Sep Purif Technol*, 2007, **55**, 212-216.
28. M. I. Amin, M. M. Ali, H. M. Kamal, A. M. Youssef and M. A. Akl, *Hydrometallurgy*, 2010, **105**, 115-119.
29. A. Drelinkiewicz, R. Laitinen, R. Kangas and J. Pursiainen, *Appl Catal a-Gen*, 2005, **284**, 59-67.
30. L. Xu, C. Basheer and H. K. Lee, *J Chromatogr A*, 2007, **1152**, 184-192.
31. J. Tan, Z. D. Liu, Y. C. Lu, J. H. Xu and G. S. Luo, *Sep Purif Technol*, 2011, **80**, 225-234.
32. W. T. Wang, R. Chen, J. H. Xu, Y. D. Wang and G. S. Luo, *Rsc Adv*, 2014, **4**, 16444-16448.
33. W. T. Wang, R. Chen, J. H. Xu, Y. D. Wang and G. S. Luo,

*Chem Eng J*, 2015, **263**, 412-418.
34. J. H. Xu, R. Chen, Y. D. Wang and G. S. Luo, *Lab Chip*, 2012, **12**, 2029-2036.
35. R. Chen, P. F. Dong, J. H. Xu, Y. D. Wang and G. S. Luo, *Lab Chip*, 2012, **12**, 3858-3860.
36. S. Torza and S. G. Mason, *Science*, 1969, **163**, 813-&.
37. W. K. Lewis and W. G. Whitman, *Ind Eng Chem*, 1924, **16**, 1215-1220.
38. M. N. Kashid, A. Renken and L. Kiwi-Minsker, *Chem Eng Sci*, 2011, **66**, 3876-3897.
39. H. Brenner, *Chem Eng Sci*, 1963, **18**, 109-122.
40. L. Oellrich, Schmidtt.H and H. Brauer, *Chem Eng Sci*, 1973, **28**, 711-721.
41. P. N. Rowe, K. T. Claxton and J. B. Lewis, *Trans Inst Chem Eng*, 1965, **43**, T14-&.
42. C. T. Culbertson, S. C. Jacobson and J. M. Ramsey, *Talanta*, 2002, **56**, 365-373.
43. C. R. Wilke and P. Chang, *Aiche J*, 1955, **1**, 264-270.